

Published in final edited form as:

*Acad Radiol.* 2012 January ; 19(1): 17–25. doi:10.1016/j.acra.2011.08.016.

## Loss of white matter microstructural integrity is associated with adverse neurological outcome in Tuberous Sclerosis Complex

Jurriaan M. Peters, MD<sup>a,b</sup>, Mustafa Sahin, MD, PhD<sup>a,\*</sup>, Vanessa K. Vogel-Farley, BSc<sup>c</sup>, Shafali S. Jeste, MD<sup>d</sup>, Charles A. Nelson III, PhD<sup>c</sup>, Matthew C. Gregas, PhD<sup>a,e</sup>, Sanjay P. Prabhu, MBBS, FRCR<sup>b</sup>, Benoit Scherrer, PhD<sup>b</sup>, and Simon K. Warfield, PhD<sup>b,\*</sup>

<sup>a</sup>Department of Neurology, Children's Hospital Boston & Harvard Medical School, 300 Longwood Avenue, Boston, MA 02115.

<sup>b</sup>Department of Radiology/Computational Radiology Laboratory, Children's Hospital Boston & Harvard Medical School, 300 Longwood Avenue, Boston, MA 02115.

<sup>c</sup>Department of Laboratories of Cognitive Neuroscience Children's Hospital Boston & Harvard Medical School, 300 Longwood Avenue, Boston, MA 02115.

<sup>d</sup>Center for Autism Research and Treatment, Semel Institute, University of California, 760 Westwood Plaza, Los Angeles, CA 90095.

<sup>e</sup>Department of Clinical Research Program, Children's Hospital Boston & Harvard Medical School, 300 Longwood Avenue, Boston, MA 02115.

### Abstract

**Rationale and Objectives**—Tuberous Sclerosis Complex (TSC) is a genetic neurocutaneous syndrome in which cognitive and social-behavioral outcomes for patients vary widely in an unpredictable manner. The cause of adverse neurological outcome remains unclear. We investigated the hypothesis that disordered white matter and abnormal neural connectivity are associated with adverse neurological outcome.

**Materials and Methods**—Structural and diffusion magnetic resonance imaging was carried out in 40 subjects with TSC (age range 0.5 – 25 years, mean age 7.2 and median age 5 years), 12 of whom had autism spectrum disorders (ASD), and in 29 age-matched controls. Tractography of the corpus callosum was used to define a 3-dimensional volume of interest. Regional averages of four diffusion scalar parameters of the callosal projections were calculated for each subject. These were the average fractional anisotropy (AFA) and average mean, radial and axial diffusivity (AMD, ARD, AAD).

**Results**—Subjects with TSC had significantly lower AFA and higher AMD, ARD and AAD values compared to controls. Subjects with TSC and ASD had significantly lower AFA values

---

© 2011 The Association of University Radiologists. Published by Elsevier Inc. All rights reserved.

\***Corresponding Authors:** Simon K. Warfield, PhD, Director, Computational Radiology Laboratory, Department of Radiology, Children's Hospital Boston, Boston, MA, Associate Professor of Radiology, Harvard Medical School, Boston, MA, 300 Longwood Avenue, Boston, MA 02115, Ph +1 617 355 2755 Fax +1 617 730 4644, simon.warfield@childrens.harvard.edu, Mustafa Sahin, MD, PhD, Director, Multi-Disciplinary Tuberous Sclerosis Program, Department of Neurology, Children's Hospital Boston, Boston, MA, Assistant Professor of Neurology, Harvard Medical School, Boston, MA, 300 Longwood Avenue, Boston, MA 02115, Ph +1 617 919 4518 Fax +1 617 730 0279, mustafa.sahin@childrens.harvard.edu.

**Publisher's Disclaimer:** This is a PDF file of an unedited manuscript that has been accepted for publication. As a service to our customers we are providing this early version of the manuscript. The manuscript will undergo copyediting, typesetting, and review of the resulting proof before it is published in its final citable form. Please note that during the production process errors may be discovered which could affect the content, and all legal disclaimers that apply to the journal pertain.

compared to those without ASD, and compared to controls. TSC subjects without ASD had similar AFA values compared to controls.

**Conclusion**—Diffusion tensor scalar parameters provided measures of properties of the three-dimensional callosal projections. In TSC, changes in these parameters may reflect microstructural changes in myelination, axonal integrity, or extracellular environment. Alterations in white matter microstructural properties were associated with TSC and larger changes were associated with TSC and ASD, thus establishing a relationship between altered white matter microstructural integrity and brain function.

---

## 1. Introduction

Tuberous Sclerosis Complex (TSC) is a genetic neurocutaneous syndrome with an estimated incidence of 1 in 6000–10,000. While some patients with TSC may never show neurological symptoms affecting their quality of life, epilepsy occurs in 80% to 90% of all patients, close to 45% of patients have mild-to-profound intellectual disabilities, and autism spectrum disorders (ASD) occurs in up to 50% of patients (1).

The cause of neurological deficits in TSC patients is a key unresolved question, and the neurological outcome remains highly variable and unpredictable. It has been hypothesized that tubers disrupt local cerebral architecture, resulting in impaired brain function. However, no robust conventional MRI measure of tubers correlates consistently with the clinical phenotype or long-term neurological outcome (2), and neither a high tuber load nor tubers in specific locations are necessary or sufficient to predict seizures, cognitive impairment, or autism (3).

More recently, investigators have studied the hypothesis that disordered white matter and abnormal neural circuitry contribute to neurological symptoms in TSC patients. Such a neural mechanism would underlie both intellectual impairment and autism, and may be responsible for comorbid autism in other disorders as well (4). Support for the existence of aberrant neural circuitry can be found in TSC mouse models. The *Tsc1* and *Tsc2* proteins appear to be crucial for proper axon specification, guidance and myelination (5–7). The neuron-specific *Tsc1* knockout mouse displays diffuse cortical and subcortical hypomyelination (6). In *Tsc2* heterozygous mice, investigators have found abnormally exuberant and disordered axonal projections from retina to the lateral geniculate nucleus, suggesting defects in axon guidance (7).

Similarly, in human subjects with TSC, Diffusion Tensor Imaging (DTI) analysis of white matter that appears normal on conventional MRI has identified abnormalities suggesting abnormal myelination and astrogliosis (8–11). Moreover, in large studies of children with *idiopathic* autism (autism with no known cause), DTI abnormalities of the corpus callosum have been identified (12, 13).

We hypothesized that disruption of the normal development of brain function in TSC patients is caused by alterations in the microstructural integrity of axons and myelination. Using DTI, we compared TSC patients with healthy controls to further characterize abnormal white matter microstructure and aberrant connectivity in TSC. In addition, we hypothesized that an increase in loss of microstructural integrity in TSC patients would lead to an increase in cognitive and social-behavioral deficits, specifically ASD. In this study we focused upon the corpus callosum, a major commissural long-distance pathway that has been well-studied in ASD as well as in TSC.

Finally, in this paper we introduce a novel tractography analysis method that considers all tractography streamlines and adjusts for partial volume averaging in the calculation of DTI measures.

## 2. Materials and Methods

### 2.1 Subjects

40 patients (age range, 0.5 – 25 years) with an established diagnosis of TSC and 29 age-matched control subjects were imaged with 3T magnetic resonance imaging. Control subjects underwent imaging as part of their routine care or as part of this research study. Each MRI was reviewed by a pediatric neuroradiologist, and all controls had a normal MRI and normal neurological examination. Controls did not undergo neuropsychological evaluation as part of this study. Recruitment of subjects and data acquisition was conducted using a protocol approved by the IRB.

All patients fulfilled the clinical criteria for definite TSC, as defined by the Tuberous Sclerosis Consensus Conference (14). All patients with TSC were neurologically examined, and clinical data were obtained during office visits and from review of medical records. ASD diagnoses were based on clinical assessment by a board certified pediatric neurologist, using the Diagnostic and Statistical Manual DSM-IV-TR (American Psychiatric Association, 2000) and in all but the three oldest subjects supported by additional testing with the Autism Diagnostic Observation Schedule (ADOS (15)) by experienced behavioral specialists.

### 2.2 Data acquisition and analysis

The MRI protocol was based on routine clinical imaging, extended with diffusion imaging. Sedation was used only in subjects undergoing clinical imaging if necessary to prevent significant motion. The imaging protocol included a T1w MPRAGE, and a T2w TSE, with diffusion imaging (16) acquired in the axial plane, utilizing 30 images with  $b=1000 \text{ s/mm}^2$  and 5  $b=0$  images (22 cm FOV, slice thickness=2.0mm, TE=88 ms, TR=10s, 128×128 matrix, 1 NEX, iPAT=2, modified as necessary to facilitate completion of the scan if the subject was unable to remain perfectly still).

A segmentation of the intracranial cavity was created from the structural MRI (17, 18). Compensation for residual distortion and patient motion was achieved by aligning the diffusion images to the T1w MPRAGE scan, with appropriate reorientation of the gradient directions (19). Tensors were estimated using robust least squares, and were displayed via color-coding (20).

We used a stochastic streamline tractography algorithm that combines the speed and efficacy of deterministic decision making at each voxel, with probabilistic sampling from the space of all streamlines. Potential streamlines are stochastically initialized and evaluated, starting from a seeding region of interest, such as all the white matter in the brain. Streamlines are initialized at stochastically sampled locations inside the seeding region-of-interest, and are constructed by stepping with sub-voxel resolution through the tensor field. For each potential streamline, we avoid loss of connectivity due to local aberrations by incorporating a low pass filter along the estimated pathway for conventional stopping criteria, including streamline curvature and fractional anisotropy criteria. The range of potential streamlines examined is broad in comparison to conventional deterministic streamline tracing, and is formed by log-Euclidean tensor interpolation (21) at each location, with stepping direction determined by a linear combination of tensor deflection (22) and primary eigenvector orientation, with stopping based on fractional anisotropy and angle criteria.

Specifically, from each stochastically selected subvoxel location  $p^k$ , a new point along the streamline is identified by stepping, with a fixed stepsize  $s$ , in the direction  $v^k$ , determined by the primary eigenvector of the tensor estimate at  $p^k$ :

$$p^{k+1} = p^k + v^k s$$

The new point  $p^{k+1}$  is tested to ensure it is inside the image boundary and inside the region to be considered for tractography. A mask can be used to ensure tractography does not step through regions with no white matter. Streamline generation is terminated if points are not validated. Streamline termination criteria related to the fractional anisotropy and angle changes are then checked. The trajectory fractional anisotropy is assessed as a linear combination of the fractional anisotropy of the tensor estimate and the previous trajectory fractional anisotropy:

$$F^{k+1} = \alpha F^k + (1 - \alpha) FA(D^{k+1})$$

where  $FA(D^{k+1})$  is the FA of the tensor  $D^{k+1}$ . The primary eigenvector of the tensor is computed, providing  $e^{k+1}$ . The angle criterion is assessed by accumulating the cosine of trajectory angle changes,  $\theta$ :

$$\theta^{k+1} = \beta \theta^k + (1 - \beta) \left( \sum_{j=1}^3 e_j^{k+1} v_k^j \right).$$

The new direction of the streamline is calculated using a combination of the primary eigenvector and tensor deflection, while accounting for the previous direction of the streamline:

$$v^{k+1} \propto \gamma v^k + (1 - \gamma) (\delta (D^{k+1})^{\epsilon} v^k + (1 - \delta) e^{k+1})$$

Propagation of each streamline was terminated if the trajectory fractional anisotropy fell below 0.15, or if the tract trajectory angle exceeded 30 degrees. The trajectories were obtained using the step size parameter  $s=0.33\text{mm}$ ,  $\alpha=0.5$ ,  $\beta=0.5$ ,  $\gamma=0.5$ ,  $\delta=0.5$ , and tensor deflection power  $\epsilon=2$ .

Furthermore, as proposed by (23), regions-of-interest may be specified to ensure potential streamlines meet requirements of known anatomy, by requiring streamlines to pass through certain regions-of-interest (selection ROIs), or requiring that they do not pass through certain regions-of-interest (exclusion ROIs). This process of stochastically sampling potential streamlines from the seeding region-of-interest enables us to identify the streamlines that are most consistent with the diffusion tensor image, even in the presence of abnormal anatomy. Stochastic sampling is continued until a predetermined number of streamlines has been examined, and each streamline meeting all criteria is stored. A streamline density image is then constructed by counting the number of times each streamline entered a voxel and dividing by the total number of streamlines.

The streamlines identified by stochastic tractography can be used to delineate a region of interest, in which the assessment of parameters of white matter microstructural integrity may be carried out. However, such an assessment can be confounded by partial volume effects

(PVE), as described by (24). When voxels associated with a fiber tract are identified, the proportion of the voxel associated with the fiber tract is important. A common strategy to select a tract-based region of interest has been to threshold the streamline density to identify voxels associated with a particular white matter (25, 26). Average parameters, such as FA or MD, characteristic of the region are then assessed by computing the mean value of the parameter by summing the parameter over all the voxels above the threshold and dividing by the number of voxels in the region (25, 26). Vos et al. (24) demonstrate that the interaction between the geometry and curvature of a white matter fascicle, and the voxel grid creates a partial volume effect that confounds the analysis. We propose to avoid the confounding due to the partial volume effect by avoiding the thresholding. Instead, we utilize the streamline density directly to enable an appropriate weighted average of diffusion tensor parameters. In our analysis, the diffusion tensor parameters of a region are calculated based on equal weighting of each of the trajectories, rather than equal weighting of each voxel. Given a streamline density image,  $d$ , and an image of a tensor scalar parameter,  $p$ , on the same discrete image lattice with voxels indexed by  $i$ , the streamline density weighted mean,  $m$ , and variance,  $v$ , of the parameter are given by :

$$m = \frac{\sum_i d_i p_i}{\sum_i d_i}, v = \frac{\sum_i d_i (p_i - m)^2}{\sum_i d_i^2}$$

The corpus callosum region-of-interest was located by inspection of the structural MRI scans and a color coded image of local tensor orientation, and delineated interactively (Figure 1A) using previously established criteria (23). The stochastic tractography was utilized to identify streamlines consistent with the projections of the corpus callosum, and are illustrated in Figure 1B. Scalar measures called Fractional Anisotropy (FA), Mean Diffusivity (MD), Axial Diffusivity (AD) and Radial Diffusivity (RD) were derived from each tensor. These measures reflect properties of the underlying white matter, but do not have high specificity for particular microstructural white matter changes (27). The streamlines passing through the corpus callosum ROI were used to construct a streamline density image, constructed by counting the number of times each trajectory entered a voxel and dividing by the total number of trajectories created, as illustrated (Figure 1C and 1D). In order to characterize the microstructural properties of the white matter of these trajectories, streamline density weighted averages of these scalar parameter values were calculated.

This provided four scalar variables characterizing the projections of the corpus callosum in each subject, the average FA (AFA), average MD (AMD), average AD (AAD) and average RD (ARD). The weighted average and variance of the fractional anisotropy (and similarly for the other scalar parameters) in the projections of the corpus callosum were computed as shown:

$$\text{AFA} = \frac{\sum_i d_i \text{FA}_i}{\sum_i d_i} \quad \text{var}(\text{AFA}) = \frac{\sum_i d_i (\text{FA}_i - \text{AFA})^2}{\sum_i d_i^2}$$

where  $i$  is the index of each voxel,  $d_i$  is the streamline density at voxel  $i$ , and  $\text{FA}_i$  is the fractional anisotropy.

Callosal volume was estimated by thresholding the streamline density image at 5% (28), counting the number of voxels and multiplying by the size of each voxel.

### 2.3 Statistical analysis

The DTI measures were treated as response variables in a regression model with age, gender, and group status. Visual plots of the data suggest that age needed to be log-transformed. This transformation was later confirmed by assessment of the value of Akaike's Information Criteria (AIC) for the models with age log-transformed and the model with age untransformed. Group status was initially defined as TSC or controls. We then refined group status into three groups: Controls, TSC with and without ASD. All two and three way interactions were considered. Interaction and main effect terms were dropped based on likelihood ratio tests so that we achieved a model that accurately described the response without extraneous terms. Group and log (age) were identified as important terms. Gender was not significant after including age and group (TSC vs. controls, or ASD/no ASD) into the model. Presence of group difference was determined by a likelihood ratio test. Significance tests were corrected for multiple comparisons (29) with a nominal alpha level of 0.05 and sequential model evaluation. Separate models were fit for each DTI measures. Models were validated through residual plots, Q-Q plots, and added variable plots.

## 3. Results

### 3.1 Patients

40 subjects (24 boys, 16 girls; mean age, 7.2 years; age range 0.5 – 25 years, median 5.0 years) underwent MR imaging. Only 1 patient had a normal MRI. 24 had clinically significant developmental delays or intellectual disability, and 12 had ASD - note that 6 patients under 1.5 years old were not considered for a formal diagnosis of ASD. 30 patients had genetic confirmation of their clinical diagnosis with abnormalities in the TSC1 (n = 8) and TSC2 (n = 22) regions, in others testing was negative or not performed (e.g. in patients with a family history of TSC). Using Fisher's Exact test, the prevalence of ASD was not significantly different in patients with TSC1 compared to TSC2 mutations ( $p = 0.4634$ ), with or without global developmental delay or mental retardation ( $p = 0.2919$ ), and with or without a family history of TSC ( $p = 0.3891$ ). Subjects with epilepsy (n = 25) and infantile spasms (n=11 out of those 25) were more likely to have ASD ( $p = 0.0132$  and  $0.0256$ , respectively).

29 age-matched controls (14 girls, 15 boys; mean age 7.7 years; age range 0.9 – 25 years, median 6.48 years) with normal MR imaging were included.

### 3.2 Diffusion tensor properties of projections of the corpus callosum

**3.2.1 TSC and controls**—Findings and p-values are presented in Table 1. Significant group differences were found, with higher AMD, AAD and ARD values in the TSC patients compared to controls. AFA differences between the TSC patients and controls were again significant ( $p = 0.035$ ) but more complex: the model fit implied that the AFA increased less with age in the TSC group than in the control group.

**3.2.2 TSC with and without ASD and controls**—Graphical displays of the linear regression model are shown (Figure 2). To summarize, significantly higher AMD, AAD, ARD values were found in TSC patients compared to control subjects, and a trend of higher AMD, AAD and ARD values in TSC patients with autism compared to those without, and to controls. Significant lower AFA values were found in TSC patients compared to controls ( $p = 0.035$ ), and appeared to be nearly solely attributable to the ASD subgroup; cases without



ASD had a similar AFA as controls ( $p = 0.8947$ ), but TSC cases with ASD had a lower AFA than controls ( $p = 0.0266$ ).

**3.2.3 Callosal volume**—Controls and TSC patients without ASD were not different in estimated volume of the corpus callosum (mean 69717 vs 64973 mm<sup>3</sup>,  $p = 0.2940$ ), but controls did differ from TSC patients with ASD (mean 54486 mm<sup>3</sup>,  $p = 0.00320$ ). This difference reached significance too between TSC patients with and without ASD ( $p = 0.0371$ ). For all subjects and controls, the volume of the corpus callosum was inversely correlated with AMD, ARD and AAD (Spearman correlation  $-0.80$ ,  $-0.73$  and  $-0.80$ , respectively,  $p < 0.000001$ ) and correlated with AFA (Spearman correlation  $0.40$ ,  $p = 0.001$ ).

## 4. Discussion

### 4.1 Relation between white matter microstructure and development of brain function

Our study provides the first imaging data that identifies an association between altered white matter microstructure and abnormal brain function in the TSC population. Moreover, a reduction in white matter integrity is seen in patients with worse neurodevelopmental outcome, i.e. in those who have ASD (Figure 3).

Several recent studies report DTI abnormalities in TSC of the normal appearing white matter (NAWM), indicating foci of microstructural abnormalities, depending on sample size and technique (8, 10, 11, 34–37) (summarized in Table 2). This body of data suggests it is likely microstructural changes are present *throughout* the cerebral WM in TSC. Our study is consistent with previous literature and is the first to allow for phenotypical correlation due to its large sample size.

In TSC, several pathophysiologic substrates have been proposed for reduced FA and increased MD in the NAWM. Changes in axonal integrity and diameter can affect *axial diffusivity* (AD) (38). *Radial diffusivity* (RD) values correlate with myelination in the normally developing mouse brain and in experimental dysmyelination (39). In our subjects, increased RD may represent disordered myelin sheaths, but also axonal depletion, or extracellular changes such as astrogliosis and giant cells (9, 10). Such changes, including abnormal neuronal organization and hypomyelination, have been shown in animal models of TSC(6). Finally, lower *fractional anisotropy* (FA) may relate to disorganized (40) and poorly myelinated (41) axons. Our findings are again in accordance with animal studies, where loss of Tsc1 or Tsc2 function has detrimental effects on regulation of axonal growth, particularly neuronal polarity and axon formation (5–7).

In idiopathic autism, the white matter appears normal on conventional imaging, but the theory of *developmental disconnection* has driven research efforts in the direction of investigating connectivity on the functional and microstructural levels. In this model, disconnection relates to impaired cortico-cortical transfer of intra- and interhemispheric information, affecting the higher order processing of complex information. In patients with ASD, these processing difficulties have been found to be consistently deficient across multiple domains and across multiple modalities (12, 42–44)

Within the white matter, the corpus callosum has been implicated in ASD in several lines of research, including imaging studies of callosal volume, white matter density, functional imaging of information transfer or resting state functional connectivity and in post-mortem studies (12, 44, 45). The corpus callosum represents a major interhemispheric tract of highly coherent white matter fibers, making it especially suited for DTI to study its microstructural connectivity as a model for disconnection in autism (12), and indeed, white matter

microstructural abnormalities have been identified with diffusion imaging in patients with idiopathic autism (46–48). Our DTI data confirm microstructural abnormalities of callosal white matter in TSC patients and more prominently in the TSC subjects with ASD, in support of the notion that abnormal white matter microstructure is related to impaired brain development and function.

Our volume estimation data is in concordance with findings of decreased callosal volume in autism in multiple imaging studies, summarized by Anderson *et al.* (45). In TSC, cortical malformations including tubers and neuronal migration defects affect white matter as migrational failure results in impaired neocortical development, which is followed by a deficiency in cortico-cortical fibers destined to be part of the corpus callosum (49, 50). In a recent study of 12 TSC patients, DTI indices of major commissural white matter also correlated with tuber load (11), suggesting more extensive malformation leading to both more tubers and decreased microstructural quality of the corpus callosum. We found significant correlations between DTI parameters and volume estimates of projections of the corpus callosum. In this interhemispheric pathway, both macrostructural and microstructural characteristics were abnormal in TSC patients with ASD.

#### 4.2 Streamline Density Weighted Statistics

There are certain artifacts and pitfalls that must be taken into consideration with respect to diffusion imaging and tractography (51). Partial volume mixing and proximity of a pathway to other pathways containing many more tracts propagating in a different direction are some of the factors that introduce errors, or even cause certain pathways to be missed completely. DTI tractography is consistent with known anatomy (23, 52), and with histological appearance of fiber structure (53, 54), but some fiber tracts are not identified and spurious fiber tracts may be incorrectly detected.

Our use of streamline density weighting compensates for partial volume averaging of fiber tracts and treats each streamline in the same way. The alternative, of identifying a region based on thresholding the streamline density, and treating each voxel equally, fails to account for the different occupancy of voxels with many streamlines in comparison to voxels with few streamlines present. In this way, we compute the mean scalar parameter of *each streamline* of a structure rather than of *each voxel*. Thus, our use of streamline density weighted statistics enables the analysis of the three-dimensional callosal projections while appropriately adjusting for changes in streamline density as well as spurious tracts. We propose our calculation of streamline density weighted averages of DTI scalar parameter values be used as a standard in the characterization of the microstructural properties of white matter fascicles.

### 5. Conclusion

Our novel method of streamline density weighted calculation of mean DTI scalar parameters allows for incorporation of all white matter projections while compensating for volume averaging, resulting in average DTI measures of a white matter structure defined by tractography rather than by its voxels. Using streamline density weighting, we found a relation between alterations in white matter microstructure and neurological outcome in TSC.

The findings of decreased AFA and increased AAD, AMD and ARD of the corpus callosum in the TSC population compared to controls, is a new finding consistent with the previous work that has identified alterations in the white matter of TSC patients. These pathological findings in the corpus callosum by DTI are likely typical of alterations *throughout* the cerebral white matter in TSC.



The significant difference of AFA between TSC subjects with and without ASD lends further support to the current hypothesis of long-range functional and structural disconnection in autism. Our finding of AFA differences raises the possibility of using callosal AFA as an early biomarker to predict ASD in the TSC population. Future longitudinal studies of our younger patients will provide much needed insights in pathologic developmental changes occurring at the critical periods in ASD (44).

## Acknowledgments

We gratefully acknowledge the contribution of MRI scans from John Gilmore and Martin Styner, supported by NIH grant P50 MH064065. The authors are indebted to the children and families who have participated in this study.

**Grant Support** M.S. is supported in part by the John Merck Fund and a Junior Investigator Award from the Children's Hospital Boston Translational Research Program. C.N. is supported by NIH grant R01 DC010290. This investigation was supported in part by NIH grant R01 RR021885, R01 LM010033, R03 EB008680 and NIH grant UL1 RR025758.

## References

1. Curatolo P, Bombardieri R, Jozwiak S. Tuberous sclerosis. *Lancet*. 2008; 372:657–668. [PubMed: 18722871]
2. Wong V. Study of the relationship between tuberous sclerosis complex and autistic disorder. *J Child Neurol*. 2006; 21:199–204. [PubMed: 16901420]
3. Jansen FE, Vincken KL, Algra A, et al. Cognitive impairment in tuberous sclerosis complex is a multifactorial condition. *Neurology*. 2008; 70:916–923. [PubMed: 18032744]
4. Clifford S, Dissanayake C, Bui QM, Huggins R, Taylor AK, Loesch DZ. Autism spectrum phenotype in males and females with fragile X full mutation and premutation. *J Autism Dev Disord*. 2007; 37:738–747. [PubMed: 17031449]
5. Choi YJ, Di Nardo A, Kramvis I, et al. Tuberous sclerosis complex proteins control axon formation. *Genes Dev*. 2008; 22:2485–2495. [PubMed: 18794346]
6. Meikle L, Talos DM, Onda H, et al. A mouse model of tuberous sclerosis: neuronal loss of Tsc1 causes dysplastic and ectopic neurons, reduced myelination, seizure activity, and limited survival. *J Neurosci*. 2007; 27:5546–5558. [PubMed: 17522300]
7. Nie D, Di Nardo A, Han JM, et al. Tsc2-Rheb signaling regulates EphA-mediated axon guidance. *Nat Neurosci*. 2010; 13:163–172. [PubMed: 20062052]
8. Arulrajah S, Ertan G, Jordan L, et al. Magnetic resonance imaging and diffusion-weighted imaging of normal-appearing white matter in children and young adults with tuberous sclerosis complex. *Neuroradiology*. 2009; 51:781–786. [PubMed: 19603155]
9. Makki MI, Chugani DC, Janisse J, Chugani HT. Characteristics of abnormal diffusivity in normal-appearing white matter investigated with diffusion tensor MR imaging in tuberous sclerosis complex. *AJNR Am J Neuroradiol*. 2007; 28:1662–1667. [PubMed: 17893226]
10. Krishnan ML, Commowick O, Jeste SS, et al. Diffusion features of white matter in tuberous sclerosis with tractography. *Pediatr Neurol*. 2010; 42:101–106. [PubMed: 20117745]
11. Simao G, Raybaud C, Chuang S, Go C, Snead OC, Widjaja E. Diffusion tensor imaging of commissural and projection white matter in tuberous sclerosis complex and correlation with tuber load. *AJNR Am J Neuroradiol*. 2010; 31:1273–1277. [PubMed: 20203114]
12. Alexander AL, Lee JE, Lazar M, et al. Diffusion tensor imaging of the corpus callosum in Autism. *Neuroimage*. 2007; 34:61–73. [PubMed: 17023185]
13. Keller TA, Kana RK, Just MA. A developmental study of the structural integrity of white matter in autism. *Neuroreport*. 2007; 18:23–27. [PubMed: 17259855]
14. Roach ES, Gomez MR, Northrup H. Tuberous sclerosis complex consensus conference: revised clinical diagnostic criteria. *J Child Neurol*. 1998; 13:624–628. [PubMed: 9881533]
15. Lord C, Risi S, Lambrecht L, et al. The autism diagnostic observation schedule-generic: a standard measure of social and communication deficits associated with the spectrum of autism. *J Autism Dev Disord*. 2000; 30:205–223. [PubMed: 11055457]

16. Reese TG, Heid O, Weisskoff RM, Wedeen VJ. Reduction of eddy-current-induced distortion in diffusion MRI using a twice-refocused spin echo. *Magn Reson Med*. 2003; 49:177–182. [PubMed: 12509835]
17. Grau V, Mewes AU, Alcaniz M, Kikinis R, Warfield SK. Improved watershed transform for medical image segmentation using prior information. *IEEE Trans Med Imaging*. 2004; 23:447–458. [PubMed: 15084070]
18. Weisenfeld NI, Warfield SK. Automatic segmentation of newborn brain MRI. *Neuroimage*. 2009; 47:564–572. [PubMed: 19409502]
19. Ruiz-Alzola J, Westin CF, Warfield SK, Alberola C, Maier S, Kikinis R. Nonrigid registration of 3D tensor medical data. *Med Image Anal*. 2002; 6:143–161. [PubMed: 12045001]
20. Douek P, Turner R, Pekar J, Patronas N, Le Bihan D. MR color mapping of myelin fiber orientation. *J Comput Assist Tomogr*. 1991; 15:923–929. [PubMed: 1939769]
21. Arsigny V, Fillard P, Pennec X, Ayache N. Log-Euclidean metrics for fast and simple calculus on diffusion tensors. *Magn Reson Med*. 2006; 56:411–421. [PubMed: 16788917]
22. Lazar M, Weinstein DM, Tsuruda JS, et al. White matter tractography using diffusion tensor deflection. *Hum Brain Mapp*. 2003; 18:306–321. [PubMed: 12632468]
23. Wakana S, Jiang H, Nagae-Poetscher LM, van Zijl PC, Mori S. Fiber tract-based atlas of human white matter anatomy. *Radiology*. 2004; 230:77–87. [PubMed: 14645885]
24. Vos SB, Jones DK, Viergever MA, Leemans A. Partial volume effect as a hidden covariate in DTI analyses. *Neuroimage*. 2011; 55:1566–1576. [PubMed: 21262366]
25. Kubicki M, Alvarado JL, Westin CF, et al. Stochastic tractography study of Inferior Frontal Gyrus anatomical connectivity in schizophrenia. *Neuroimage*. 2011; 55:1657–1664. [PubMed: 21256966]
26. Powell HW, Parker GJ, Alexander DC, et al. Hemispheric asymmetries in language-related pathways: a combined functional MRI and tractography study. *Neuroimage*. 2006; 32:388–399. [PubMed: 16632380]
27. Basser PJ, Pierpaoli C. Microstructural and physiological features of tissues elucidated by quantitative-diffusion-tensor MRI. *J Magn Reson B*. 1996; 111:209–219. [PubMed: 8661285]
28. Chung HW, Chou MC, Chen CY. Principles and limitations of computational algorithms in clinical diffusion tensor MR tractography. *AJNR Am J Neuroradiol*. 2011; 32:3–13. [PubMed: 20299436]
29. Ge Y, Sealfon SC, Speed TP. Some Step-Down Procedures Controlling the False Discovery Rate under Dependence. *Statistica Sinica*. 2008; 18:881–904. [PubMed: 19018297]
30. Gillberg IC, Gillberg C, Ahlsen G. Autistic behaviour and attention deficits in tuberous sclerosis: a population-based study. *Dev Med Child Neurol*. 1994; 36:50–56. [PubMed: 8132114]
31. Numis AL, Major P, Montenegro MA, Muzykewicz DA, Pulsifer MB, Thiele EA. Identification of risk factors for autism spectrum disorders in tuberous sclerosis complex. *Neurology*. 2011; 76:981–987. [PubMed: 21403110]
32. O'Callaghan FJ, Harris T, Joinson C, et al. The relation of infantile spasms, tubers, and intelligence in tuberous sclerosis complex. *Arch Dis Child*. 2004; 89:530–533. [PubMed: 15155396]
33. Curatolo P, Porfirio MC, Manzi B, Seri S. Autism in tuberous sclerosis. *Eur J Paediatr Neurol*. 2004; 8:327–332. [PubMed: 15542389]
34. Widjaja E, Simao G, Mahmoodabadi SZ, et al. Diffusion tensor imaging identifies changes in normal-appearing white matter within the epileptogenic zone in tuberous sclerosis complex. *Epilepsy Res*. 89:246–253. [PubMed: 20129760]
35. Garaci FG, Floris R, Bozzao A, et al. Increased brain apparent diffusion coefficient in tuberous sclerosis. *Radiology*. 2004; 232:461–465. [PubMed: 15215545]
36. Peng SS, Lee WT, Wang YH, Huang KM. Cerebral diffusion tensor images in children with tuberous sclerosis: a preliminary report. *Pediatr Radiol*. 2004; 34:387–392. [PubMed: 15029464]
37. Luat AF, Makki M, Chugani HT. Neuroimaging in tuberous sclerosis complex. *Curr Opin Neurol*. 2007; 20:142–150. [PubMed: 17351483]

38. Budde MD, Xie M, Cross AH, Song SK. Axial diffusivity is the primary correlate of axonal injury in the experimental autoimmune encephalomyelitis spinal cord: a quantitative pixelwise analysis. *J Neurosci*. 2009; 29:2805–2813. [PubMed: 19261876]
39. Song SK, Yoshino J, Le TQ, et al. Demyelination increases radial diffusivity in corpus callosum of mouse brain. *Neuroimage*. 2005; 26:132–140. [PubMed: 15862213]
40. Beaulieu C, Allen PS. Determinants of anisotropic water diffusion in nerves. *Magn Reson Med*. 1994; 31:394–400. [PubMed: 8208115]
41. Gulani V, Webb AG, Duncan ID, Lauterbur PC. Apparent diffusion tensor measurements in myelin-deficient rat spinal cords. *Magn Reson Med*. 2001; 45:191–195. [PubMed: 11180424]
42. Geschwind DH, Levitt P. Autism spectrum disorders: developmental disconnection syndromes. *Curr Opin Neurobiol*. 2007; 17:103–111. [PubMed: 17275283]
43. Minshew NJ, Williams DL. The new neurobiology of autism: cortex, connectivity, and neuronal organization. *Arch Neurol*. 2007; 64:945–950. [PubMed: 17620483]
44. Courchesne E, Pierce K, Schumann CM, et al. Mapping early brain development in autism. *Neuron*. 2007; 56:399–413. [PubMed: 17964254]
45. Anderson JS, Druzgal TJ, Froehlich A, et al. Decreased interhemispheric functional connectivity in autism. *Cereb Cortex*. 2011; 21:1134–1146. [PubMed: 20943668]
46. Jou RJ, Jackowski AP, Papademetris X, Rajeevan N, Staib LH, Volkmar FR. Diffusion tensor imaging in autism spectrum disorders: preliminary evidence of abnormal neural connectivity. *Aust N Z J Psychiatry*. 2011; 45:153–162. [PubMed: 21128874]
47. Lange N, Dubray MB, Lee JE, et al. Atypical diffusion tensor hemispheric asymmetry in autism. *Autism Res*. 2010; 3:350–358. [PubMed: 21182212]
48. Shukla DK, Keehn B, Lincoln AJ, Muller RA. White matter compromise of callosal and subcortical fiber tracts in children with autism spectrum disorder: a diffusion tensor imaging study. *J Am Acad Child Adolesc Psychiatry*. 2010; 49:1269–1278. 1278 e1261–1262. [PubMed: 21093776]
49. Volpe, JJ. *Neurology of the newborn*. Philadelphia: Saunders; 2008.
50. Widjaja E, Blaser S, Miller E, et al. Evaluation of subcortical white matter and deep white matter tracts in malformations of cortical development. *Epilepsia*. 2007; 48:1460–1469. [PubMed: 17441991]
51. Le Bihan D, Poupon C, Amadon A, Lethimonnier F. Artifacts and pitfalls in diffusion MRI. *J Magn Reson Imaging*. 2006; 24:478–488. [PubMed: 16897692]
52. Zhang Y, Zhang J, Oishi K, et al. Atlas-guided tract reconstruction for automated and comprehensive examination of the white matter anatomy. *Neuroimage*. 52:1289–1301. [PubMed: 20570617]
53. Dauguet J, Peled S, Berezovskii V, et al. Comparison of fiber tracts derived from in-vivo DTI tractography with 3D histological neural tract tracer reconstruction on a macaque brain. *Neuroimage*. 2007; 37:530–538. [PubMed: 17604650]
54. Leergaard TB, White NS, de Crespigny A, et al. Quantitative histological validation of diffusion MRI fiber orientation distributions in the rat brain. *PLoS One*. 5:e8595. [PubMed: 20062822]

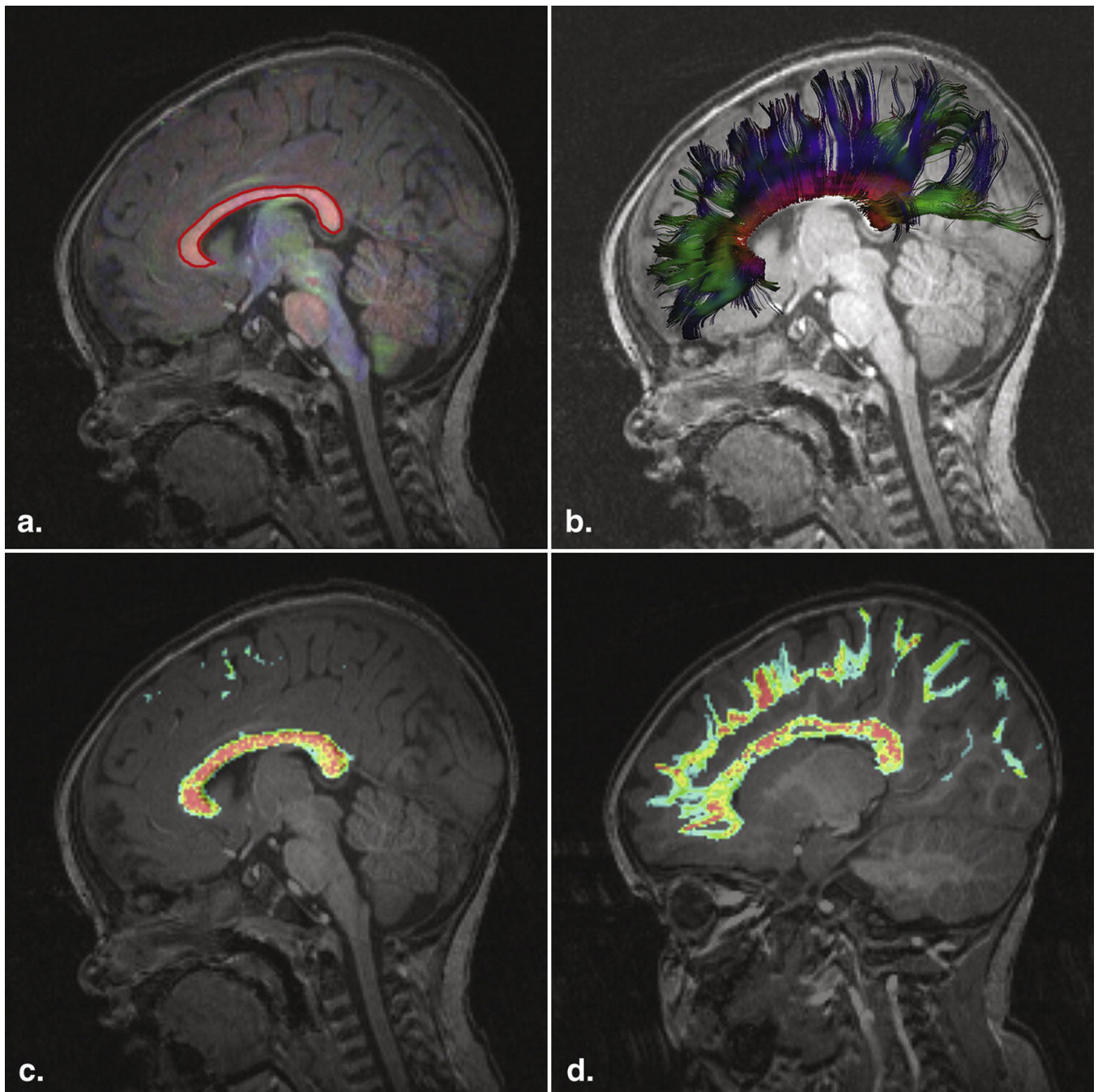


**Figure 1.**

(A) T1-weighted image, superimposed color coded representation of tensors, intensity proportional to the fractional anisotropy. Red for left-right, blue for superior-inferior, green for anterior-posterior. A manually drawn two-dimensional ROI delineates the corpus callosum (CC). (B) Visualization of the color-coded tractography of the CC. (C) Streamline Density weighted image of the CC. Red (high) and blue (low) colors represent streamline density at each voxel. (D) Out of the midsagittal plane, the streamline density weighted map follows the trajectories to the cortex.



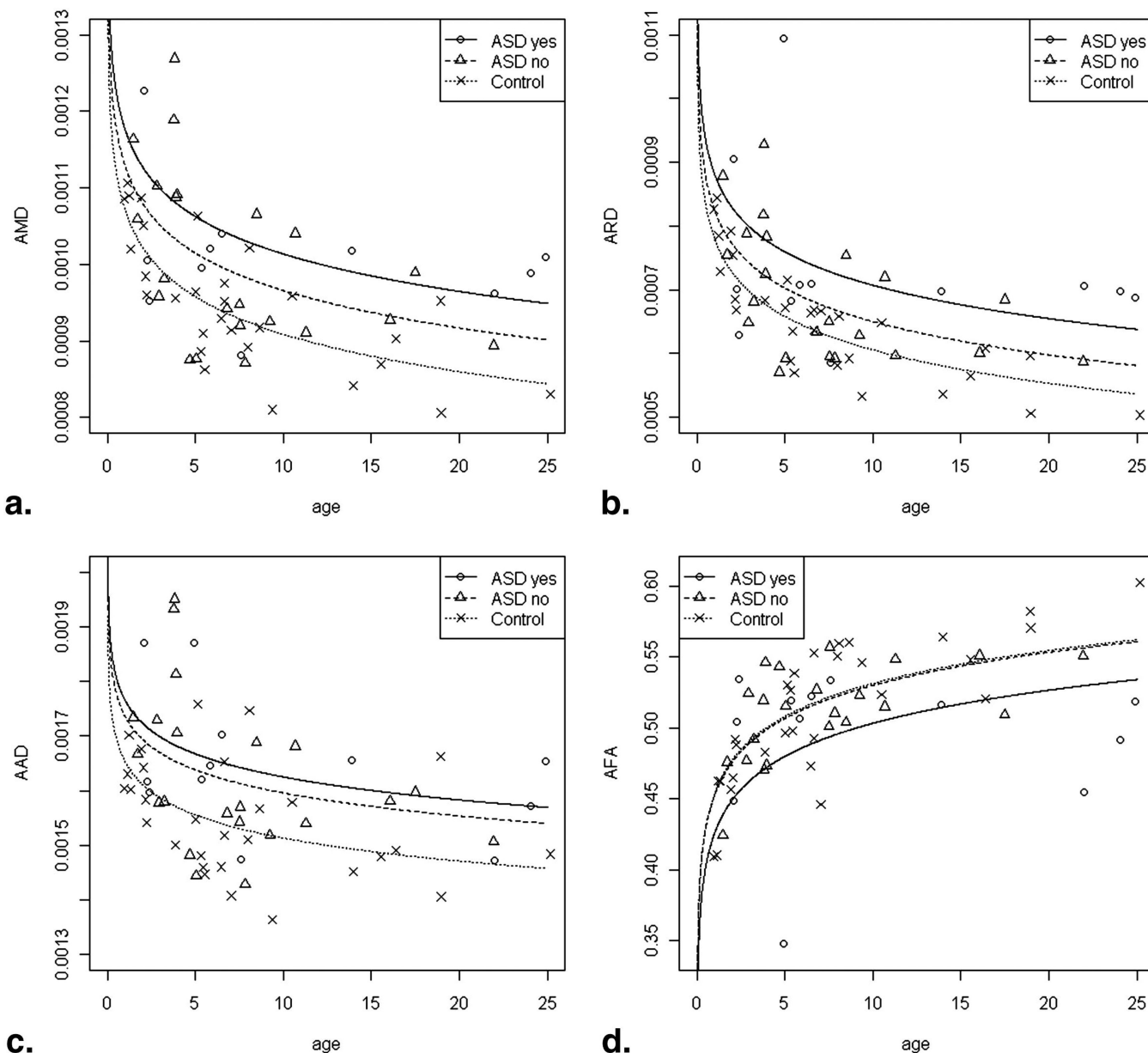


**Figure 2.** (A–C) Graphical displays of the fit linear regression model for AMD (A), ARD (B) and AAD (C). Controls (dotted line) have lower AMD, ARD and AAD than TSC patients with ASD (solid line), but this difference only reaches significance for AMD and AAD when controls are compared to TSC patients without ASD (dashed line). For AFA (D), controls and TSC without ASD have highly similar values. AFA of the TSC patients with ASD are significantly lower than controls and TSC patients without ASD.

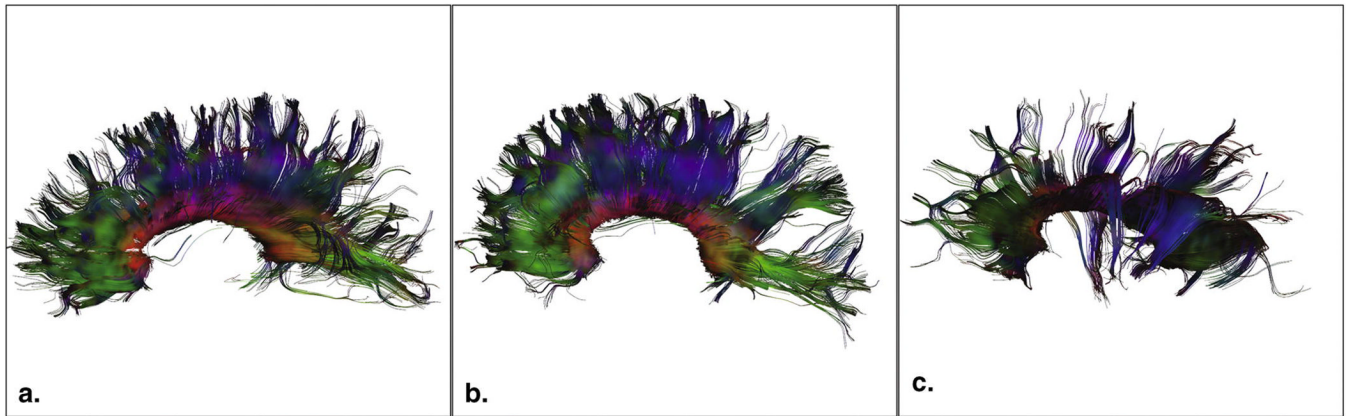


**Figure 3.** Illustration of projections of the corpus callosum and AFA values. (A) 5.3 year-old healthy control, AFA = 0.53. (B) 4.7 year-old with TSC but no ASD, AFA = 0.54 and (C) 4.9 year old with TSC and autism, AFA = 0.34



**Table 1**

*p*-values using the linear regression model with the DTI measure as the response and group (control, TSC, TSC without ASD, TSC with ASD) and log(age) as the predictors

	<b>Controls – TSC (all cases)</b>	<b>Controls – TSC without ASD</b>	<b>Controls – TSC with ASD</b>	<b>TSC without ASD – TSC with ASD</b>
AMD	0.000652	0.022068	0.000807	0.128267 (NS)
ARD	0.00200	0.062096 (NS)	0.000764	0.060672 (NS)
AAD	0.000876	0.011224	0.005148	0.467143 (NS)
AFA	0.0350	0.8947 (NS)	0.0266	0.0421

All four DTI measures differed significantly between controls and TSC patients. The AFA was significantly lower in the TSC subjects with ASD compared to those without ASD, but no difference was found between TSC patients without ASD and controls.

Table 2

Summary of published DTI studies involving NAWM in TSC

Author, year	N	Age mean, range (year)	MRI	Directions	Key findings – TSC compared to controls unless otherwise stated
Garaci 2004 (29)	18	20, 12 – 30	1.5T	6	MD of perilesional NAWM higher than contralateral NAWM. NAWM of frontal, occipital and parietal regions and CS higher MD than controls.
Peng 2004 (30)	7	-, 0.5 – 15	1.5T	6	Lower FA of WM lesions associated with tubers vs. contralateral NAWM. Higher MD of CR and SS vs. controls. Increased $\lambda_3$ of ILF and SS vs. controls.
Karadag 2005 (43)	7	-, 2 – 20	1.5T	6	Higher MD of tubers vs. cortex of controls. Increased MD and lower FA in WM lesions and perilesional WM vs. controls. No difference in MD and FA of NAWM vs. controls.
Firat 2006 (44)	6	9, 3 – 15	1.5T	6	MD of tubers higher than NAWM. MD of NAWM not different from controls.
Makki 2007 (9)	6	10, 6 – 15	1.5T	6	Higher MD, lower FA in combined NAWM of genu/splenium CC. IC/EC vs. controls. Greatest increase was in $\lambda_{2,3}$ (i.e. RD).
Aruljajah 2009 (8)	23	12, 1 – 25	1.5T	3–18	Increased MD of frontal and pontine NAWM (in subgroup 8–12 year), right parietal and occipital NAWM (in subgroup >12 year) vs. controls.
Krishnan 2010 (10)	10	-, 1.5 – 25	3T	35	Lower FA in splenium CC and GCT, lower AD in IC, STG and GCT, increased MD and RD in splenium CC of TSC vs. controls.
Simao 2010 (11)	12	9, 5 – 16	3T	15	Increased MD, decreased FA, increased RD in genu and splenium CC. Increased MD in IC. DTI measures of genu and splenium CC correlate with tuber volume (not number).
Peters, <i>this study</i>	40	7, 0.5 – 25	3T	35	Lower FA, higher MD, RD, AD of entire CC in TSC (all) vs. controls and TSC (with ASD) vs. controls. Lower FA of CC in TSC with ASD vs. TSC without ASD. No difference in FA of CC in TSC without ASD vs. controls.

CC = corpus callosum, CR = corona radiata, CSO = centrum semiovale, CST = corticospinal tract, EC = external capsule, GCT = geniculocalcarine tract, IC = internal capsule, ILF = inferior longitudinal fasciculus, NAWM = normal appearing white matter, SS = sagittal striatum, STG = superior temporal gyrus.

MD = Mean Diffusivity, RD = Radial Diffusivity, AD = Axial Diffusivity, FA = fractional anisotropy, TSC = Tuberous Sclerosis, ASD = Autism Spectrum Disorder